

# A search for rotating radio transients and fast radio bursts in the Parkes high-latitude pulsar survey

A. Rane<sup>1</sup>, D. R. Lorimer<sup>1,2</sup>, S. D. Bates<sup>2</sup>, N. McMann<sup>1</sup>, M. A. McLaughlin<sup>1</sup>  
and K. Rajwade<sup>1</sup>

<sup>1</sup>*Department of Physics & Astronomy, West Virginia University, Morgantown, WV, 26506 USA*

<sup>2</sup>*National Radio Astronomy Observatory, PO Box 2, Green Bank, WV 24944, USA*

6 February 2022

## ABSTRACT

Discoveries of rotating radio transients and fast radio bursts (FRBs) in pulsar surveys suggest that more of such transient sources await discovery in archival data sets. Here we report on a single-pulse search for dispersed radio bursts over a wide range of Galactic latitudes ( $|b| < 60^\circ$ ) in data previously searched for periodic sources by Burgay et al. We re-detected 20 of the 42 pulsars reported by Burgay et al. and one rotating radio transient reported by Burke-Spolaor. No FRBs were discovered in this survey. Taking into account this result, and other recent surveys at Parkes, we corrected for detection sensitivities based on the search software used in the analyses and the different backends used in these surveys and find that the all-sky FRB event rate for sources with a fluence above 4.0 Jy ms at 1.4 GHz to be  $\mathcal{R} = 4.4^{+5.2}_{-3.1} \times 10^3$  FRBs day<sup>-1</sup> sky<sup>-1</sup>, where the uncertainties represent a 99% confidence interval. While this rate is lower than inferred from previous studies, as we demonstrate, this combined event rate is consistent with the results of all systematic FRB searches at Parkes to date and does not require the need to postulate a dearth of FRBs at intermediate latitudes.

**Key words:** surveys methods: data analysis (stars:) pulsars: general

## 1 INTRODUCTION

The radio transient sky contains a number of known and potential classes of sources which emit on timescales ranging from nanoseconds to years. These classes include the Sun, planets, brown dwarfs, flare stars, X-ray binaries, ultra-high energy particles, magnetars,  $\gamma$ -ray bursts, maser flares, active galactic nuclei, radio supernovae, pulsars, annihilating black holes, and transmissions from extraterrestrial civilizations (for a review, see, e.g., Cordes et al. 2004, Lazio 2012). Recently Pietka et al. (2015) have analyzed the variability timescales of radio flares from nearly 90 different objects/events varying from flare stars to supermassive black holes in active galactic nuclei and have demonstrated that variability timescales could be used as an early diagnostic of source class in future radio transient surveys.

Within the last decade, as part of the analyses of pulsar surveys, a new transient phenomenon — known as fast radio bursts (FRBs) — has been identified. FRBs are categorized as short duration (few ms) bursts that are non-repeating with dispersion measures higher than the Galactic dispersion measure (DM) expected along that direction (Cordes & Lazio 2002). The DMs range from 300–1600 cm<sup>-3</sup> pc and have so far only been

observed in the 1–2 GHz band. To date, 11 FRBs have been published<sup>1</sup> (Lorimer et al. 2007; Keane et al. 2012; Thornton et al. 2013; Thornton 2013; Spitler et al. 2014; Burke-Spolaor & Bannister 2014; Petroff et al. 2015a; Ravi et al. 2014). Although, most of these were discovered in archival surveys, FRB 140514 (Petroff et al. 2015a) and FRB 131104 (Ravi et al. 2014) are real-time discoveries with a transient pipeline developed at the Parkes telescope. Despite a significant amount of follow-up observations which closely followed FRB 140514 (Petroff et al. 2015a), and inspection of archival surveys for other FRBs, none of the FRBs currently known are associated with any source counterpart at other wavelengths.

As remarked by many authors, the high DMs of FRBs are suggestive of an extragalactic origin. Among the proposed extragalactic source populations for FRBs are annihilating black holes (Keane et al. 2012), flaring magnetars (Popov & Postnov 2013), binary white dwarf mergers (Kashiyama et al. 2013), binary neutron star mergers (Totani 2013), collapsing neutron stars

<sup>1</sup> For an updated list, see <http://astro.phys.wvu.edu/FRBs>

(Falcke & Rezzolla 2014), and neutron star-black hole mergers (Lipunov & Pruzhinskaya 2014).

In view of the lack of any extragalactic counterparts identified so far, a number of other scenarios remain equally intriguing. Loeb et al. (2014) considered the case of nearby Galactic flaring main-sequence stars within 1 kpc as the sources of FRBs. They propose that the excess dispersion comes from propagation through the stellar corona. However Luan & Goldreich (2014) argued that the free-free absorption would conceal any radio signal emitted from below the corona. Also, FRBs exhibit quadratic dispersion curves that are consistent with the assumption of weak dispersion in a low density plasma. So, for the above model, in which the dispersion is concentrated in a relatively high density region, the quadratic dispersion approximation breaks down as the plasma frequency is comparable to the propagation frequency, posing significant problems for this model (Dennison 2014). However, Maoz et al. (2015) have recently found possible flare stars in additional FRB fields using time-domain optical photometry and spectroscopy. The authors have evaluated the chance probabilities of these possible associations to be in the range 0.1% to 9%. FRB 140514 was discovered in the radio follow-up observations of FRB 110220, three years apart within the same radio beam. Maoz et al. (2015) also claim that these two FRBs are from the same repeating source with 99% confidence and are consistent with the flare-star scenario with a varying plasma blanket between bursts. More FRB detections in general are necessary to confirm or refute a Galactic origin of FRBs.

Although FRBs have so far been observed over a range of Galactic latitudes, their true distribution on the sky remains unclear. Recently, based on an analysis of Parkes High Time Resolution Universe (HTRU) mid-latitude survey data, Petroff et al. (2014) proposed that there is a deficit of FRBs at intermediate latitudes. Further analyses of archival and current surveys are required to investigate this issue. In addition, Keane & Petroff (2015) have assessed the commonly used search algorithms used for FRB searches which impact the FRB sensitivities in individual surveys. Motivated by these results, in this paper we present a single-pulse search which is sensitive to both RRATs (McLaughlin et al. 2006) and FRBs on archival data previously searched for pulsars at high Galactic latitudes by Burgay et al. (2006). In § 2 we outline the basic methodology behind the search and the detection criteria. Our results and single-pulse statistics of known pulsars re-detected in this search are discussed in § 3. In § 4 we use our non-detection of FRBs to constrain their all-sky event rate. Finally, in § 5 we summarize our results and present our conclusions.

## 2 SEARCH METHODS AND ANALYSIS

### 2.1 Survey parameters

The Parkes high-latitude (PH) survey (Burgay et al. 2006) was designed to find millisecond pulsars and exotic binaries which migrate away from the Galactic plane. A total of 42 pulsars were detected in this survey, of which seven were millisecond pulsars and 18 were new discoveries. The analysis of the data by Burgay et al. (2006) was carried out using the standard periodicity search methods to find periodic signals. However no single-pulse searches have been

published on these data. The single-pulse search method is very effective in detecting sporadic sources like some pulsars (e.g. nulling pulsars) and RRATs in the time domain since these might not be detectable in the standard periodicity searches (Cordes & McLaughlin 2003). Moreover, FRBs can of course only be detected through single-pulse searches (see below § 2.2.2).

The PH survey covered a strip of the sky enclosed by Galactic longitudes  $220^\circ \leq l \leq 260^\circ$  and Galactic latitudes  $|b| \leq 60^\circ$  corresponding to a total sky coverage of  $3588 \text{ deg}^2$  in 475 hours. The survey began in November 2000 and ended in December 2003 and made use of the 13-beam receiver on the Parkes 64-m radio telescope. Data were collected simultaneously by 13 beams at a central frequency of 1374 MHz with 96 frequency channels, each 3 MHz wide. Each of the 6456 pointings was observed for 265 s. For more details about the receiver system and data acquisition, see Burgay et al. (2006).

### 2.2 Single-pulse search method

Each of these beams from the survey was processed independently using the SIGPROC software package<sup>2</sup>. The steps included in our analysis are:

- (i) dedisperse the raw data file at a range of trial DM values and remove radio frequency interference (RFI) at zero DM;
- (ii) search for individual pulses in the time series above signal-to-noise (S/N) of five and with different widths;
- (iii) apply the detection criteria to filter in terms of DM, S/N, and number of beams;
- (iv) manually inspect the resulting diagnostic plots.

We describe each step in detail below, and give the appropriate SIGPROC modules used.

#### 2.2.1 Dedispersion

Radio signals are affected by interstellar dispersion, and as a result, the higher frequencies of the signal traveling faster through the interstellar medium arrive earlier than their lower frequency counterparts. The time delay between the two frequencies  $f_1$  and  $f_2$ , (see, e.g., Lorimer & Kramer 2004) is

$$\Delta t \simeq 4150 \text{ s} \left[ \left( \frac{f_1}{\text{MHz}} \right)^{-2} - \left( \frac{f_2}{\text{MHz}} \right)^{-2} \right] \left( \frac{\text{DM}}{\text{cm}^{-3} \text{ pc}} \right), \quad (1)$$

where DM is the integrated number density of free electrons along the line of sight. This dispersion allows us to distinguish between astrophysical and terrestrial signals. It causes a quadratic sweep across the band and may be removed by appropriately shifting the frequency channels. Each time series was dedispersed over a range of trial DM values using the **dedisperse** routine in SIGPROC. For this analysis, we have searched DMs in a range from  $0 - 10^4 \text{ cm}^{-3} \text{ pc}$ . The wide range of DM makes the search sensitive to events that are highly dispersed. The trial DM step sizes used in the analysis were calculated using an algorithm, **dedisperse\_all**, originally described by Levin (2012) which accounts for the

<sup>2</sup> <http://sigproc.sourceforge.net>

amount of pulse broadening caused by the size of the previous DM step and then determines the next trial DM. A total pulse width smearing due to the DM step in comparison to the value at the last DM is chosen to be 25% (see, § Appendix). The total number of DMs searched was 249, as chosen optimally by this program. For the DM steps used in our analysis, the average S/N loss is  $\sim 1.5\%$  for DMs  $< 2000 \text{ cm}^{-3} \text{ pc}$  and for DMs between  $2000\text{--}10000 \text{ cm}^{-3} \text{ pc}$ , the average S/N loss is  $\sim 2.5\%$ , calculated using Equations 12 and 13 of Cordes & McLaughlin (2003). The `dedisperse` routine uses Equation 1 to calculate the time delays for each test DM and applies to frequency channels and the samples from each channel are then averaged to form a dedispersed time series. In addition to this, it also performs zero-DM subtraction (Eatough et al. 2009) on the time series to remove any RFI at zero DM.

### 2.2.2 Single-pulse search

Each dedispersed time series corresponding to a particular trial DM was searched for transient events of different widths via the matched filtering technique for top-hat pulses implemented in the program `seek`. This simple algorithm, which is an implementation of the method described in Cordes & McLaughlin (2003), saves individual events that deviate by five standard deviations from the mean of the time series. A number of adjacent samples are added to search for pulses of different widths. Each time series was smoothed 15 times, corresponding to a maximum smoothing of  $2^{15}$  times the sampling interval, i.e. pulse widths out to 4.096 s. If a pulse is detected in more than one of the smoothed times series, only the highest S/N value is recorded. Following Burke-Spolaor et al. (2011), the number of independent trials

$$N = N_{\text{DM}} \sum_{j=0}^{j_{\text{max}}} \frac{N_{\text{samp}}}{2^j}, \quad (2)$$

where  $N_{\text{DM}}$  is the number of DM trials,  $N_{\text{samp}}$  is the number of samples in each dedispersed time series, and  $j_{\text{max}}$  corresponds to number of matched-filter widths used. We find  $N = 1.1 \times 10^9$  for our observation. For more details of this search method, see Cordes & McLaughlin (2003).

Keane & Petroff (2015) have assessed the performance of the search algorithms commonly being used to discover FRBs. The authors point out some important concerns where sensitivity to FRBs is often unnecessarily reduced and that the single-pulse search routines within the `dedisperse_all` and `seek` packages were less efficient compared to `Heimdall` and `destroy` packages (see, e.g., Petroff et al. 2014). Based on the simulations which used an injected signal of known strength, Keane & Petroff (2015) demonstrated that the recovered S/N for `dedisperse_all` and `seek` was a function of pulse phase. We apply these results into our analysis, as described in § 4.

### 2.2.3 Detection criteria

These dispersed pulses can be displayed graphically using the `plotpulses` program and the resulting single-pulse plot can be seen in the left panel of Fig. 1. In the DM histogram, we are able to detect sources that emit many weak pulses.

Such sources might not be detectable in the bottom plot. Conversely, the sources that emit only a few strong pulses may only be detectable in the bottom plot. Often a peak in the DM histogram at low DMs is seen which is indicative of RFI. In some cases, RFI is seen at all DMs for a certain time range which can further limit our ability to detect a transient event. This would happen if there is a strong source of RFI that causes the receiver to saturate or some other local interference that is so strong that it shows up at all DMs for that time range. The single-pulse plots thus obtained were inspected manually (e.g. by searching for a well-defined peak in the S/N versus DM plot, see Fig. 1). For manual inspection, we restricted the S/N threshold to six in order to keep the number of potential candidates at a manageable level.

The event detected by Lorimer et al. (2007) was detected simultaneously in three beams and all of the other FRBs were detected in only a single beam. A strong signal appearing in all 13 beams simultaneously showing a dispersive delay is considered to have a terrestrial or instrumental origin (called perytons, Burke-Spolaor et al. 2011). The origin of these events has been recently identified as coming from a microwave oven when its door is opened prematurely and if the telescope is at an appropriate relative angle at that time (Petroff et al. 2015b). We did not detect any such events in our analysis. We found a number of bursts with high S/N in all 13 beams but no dispersive delay in the frequency versus time plot. These events are sources of RFI which have near earth origin and are only active for a brief period of time. Nearly 10% of the data show S/N greater than six in more than five beams but do not show dispersive delay. We did not consider these candidates further in our analysis.

### 2.2.4 Manual inspection

The diagnostic plots obtained after applying all the detection criteria were manually examined to look for a strong signal corresponding to a peak in the S/N versus DM plot. Such candidates are shortlisted and the detection is confirmed if the signal shows a sweep from high to low frequency across the observing bandwidth in the frequency versus time plot. Brightness was not a criterion for being shortlisted and some candidates were confirmed as pulsars despite not being detectable in this plot. For FRBs, if a dispersive sweep is absent then it is deemed to be a “false detection” (see, e.g., Fig. 2). A burst-like event was seen in one of the beams (see a bright pulse in the lower plot of Fig. 2 and a corresponding peak in the S/N versus DM plot in the upper right plot) but no dispersed signal was detected in the frequency versus time plot (see right panel of Fig. 2).

## 3 RESULTS

As summarized in Table 1, our single-pulse search resulted in the detection of 20 of the 42 pulsars detected in the original periodicity search by Burgay et al. (2006). In addition, one RRAT not reported by Burgay et al. (2006) was detected. The discovery of this source, PSR J0410–3113, was reported by Burke-Spolaor et al. (2011) during a single-pulse search on the data obtained from the high-latitude HTRU survey.

**Table 1.** All pulsars detected and discovered in the PH survey. Columns 1 to 5 report the pulsar name, Galactic longitude and latitude, spin period, and DM, all obtained from the ATNF pulsar catalog (Manchester et al. 2005). For those that were detected in our single-pulse search method, columns 6, 7, 8, and 9 report the DM obtained in this analysis, peak S/N from single-pulse search, number of pulses, and width. Column 10 lists S/N from the periodicity search obtained from Burgay et al. (2006) and column 11 lists the intermittency measure. The RRAT discovered by Burke-Spolaor et al. (2011) and re-detected in our analysis is denoted by \*.

Name PSR	$l$ ( $^{\circ}$ )	$b$ ( $^{\circ}$ )	$P$ (ms)	$DM$ (pc cm $^{-3}$ )	$DM_{\text{obs}}$ (pc cm $^{-3}$ )	$(S/N)_{\text{SP}}$	$N_{\text{pulses}}$	$W$ (ms)	$(S/N)_{\text{per}}$	$r$
J0343–3000	227.76	–52.34	2597.02	20.2	22.3	21.5	22	2.0	42.7	0.50
J0410–3113*	253.47	–41.95	1837.00	9.9	9.9	9.2	1	4.0	–	–
J0437–4715	253.47	–41.95	5.70	2.6	2.6	12.8	4303	0.3	603.3	0.02
J0448–2749	228.43	–37.91	450.40	26.2	26.4	10.2	6	4.0	28.5	0.38
J0520–2553	228.51	–30.53	241.60	33.7	–	–	–	–	34.0	–
J0610–2100	227.75	–18.18	3.86	60.6	–	–	–	–	10.1	–
J0630–2834	237.03	–16.75	1244.40	34.5	35.3	20.2	63	16.0	277.4	0.07
J0633–2015	229.33	–12.95	3253.21	90.7	89.7	11.0	3	8.0	16.4	0.67
J0636–4549	254.55	–21.55	1984.59	26.3	–	–	–	–	11.2	–
J0656–2228	233.66	–8.98	1224.75	32.4	31.1	6.9	29	0.3	21.0	0.33
J0719–2545	238.93	–5.83	974.72	253.9	–	–	–	–	20.7	–
J0726–2612	240.08	–4.64	3442.31	69.4	68.8	16.8	9	4.0	15.1	1.11
J0729–1448	230.46	1.44	251.60	92.3	–	–	–	–	32.5	–
J0729–1836	233.83	–0.33	510.10	61.2	61.0	7.4	26	0.3	59.3	0.13
J0737–3039A	245.24	–4.50	22.70	48.9	–	–	–	–	18.7	–
J0737–3039B	245.24	–4.50	2773.46	48.9	–	–	–	–	–	–
J0738–4042	254.27	–9.1	374.90	160.8	161.3	20.8	644	2.0	542.1	0.04
J0742–2822	243.85	–2.43	166.70	73.8	73.0	18.3	2130	2.0	63.1	0.29
J0746–4529	259.20	–10.10	2791.03	134.6	–	–	–	–	10.3	–
J0749–4247	257.14	–8.33	1095.40	104.5	–	–	–	–	17.6	–
J0758–1528	234.54	7.24	682.20	63.3	62.9	13.4	67	8.0	99.0	0.14
J0818–3232	251.36	1.87	2161.26	131.8	–	–	–	–	27.3	–
J0820–1350	235.96	12.61	1238.10	40.9	39.9	19.0	28	16.0	112.5	0.17
J0820–3921	257.26	–1.58	1073.57	179.4	–	–	–	–	13.4	–
J0820–4114	258.82	–2.72	545.40	113.4	–	–	–	–	42.6	–
J0821–4221	259.83	–3.14	396.73	270.6	–	–	–	–	10.8	–
J0823+0159	222.06	21.26	864.80	23.7	22.3	15.8	54	8.0	13.1	1.21
J0828–3417	254.04	2.58	1848.90	52.2	52.5	13.3	5	–	49.2	0.27
J0835–3707	257.15	2.00	541.40	112.3	113.5	6.9	1	8.0	33.2	0.21
J0837–4135	260.98	–0.32	751.60	147.3	147.8	23.2	303	4.0	152.2	0.15
J0838–2621	248.81	8.98	308.58	116.9	–	–	–	–	9.6	–
J0843+0719	219.40	28.22	1365.86	36.6	–	–	–	–	15.9	–
J0846–3533	257.26	4.72	1116.00	94.1	–	–	–	–	103.1	–
J0855–3331	256.92	7.53	1267.50	86.6	89.7	9.9	12	8.0	42.5	0.23
J0900–3144	256.16	9.49	11.11	75.7	–	–	–	–	20.8	–
J0908–1739	246.19	19.86	401.60	15.8	–	–	–	–	23.9	–
J0922+0638	225.48	36.40	430.60	27.3	26.4	18.2	195	4.0	96.8	0.19
J0944–1354	249.20	28.86	570.20	12.4	–	–	–	–	43.1	–
J0953+0755	228.97	43.71	253.00	2.9	3.0	14.0	657	2.0	128.7	0.11
J1022+1001	231.86	51.11	16.40	10.3	10.4	9.6	266	0.5	318.7	0.03
J1024–0719	251.77	40.53	5.10	6.4	–	–	–	–	33.4	–
J1038+0032	247.15	48.47	28.85	26.6	–	–	–	–	18.1	–
J1046+0304	246.48	51.71	326.20	25.3	28.2	9.8	1	8.0	25.5	0.38

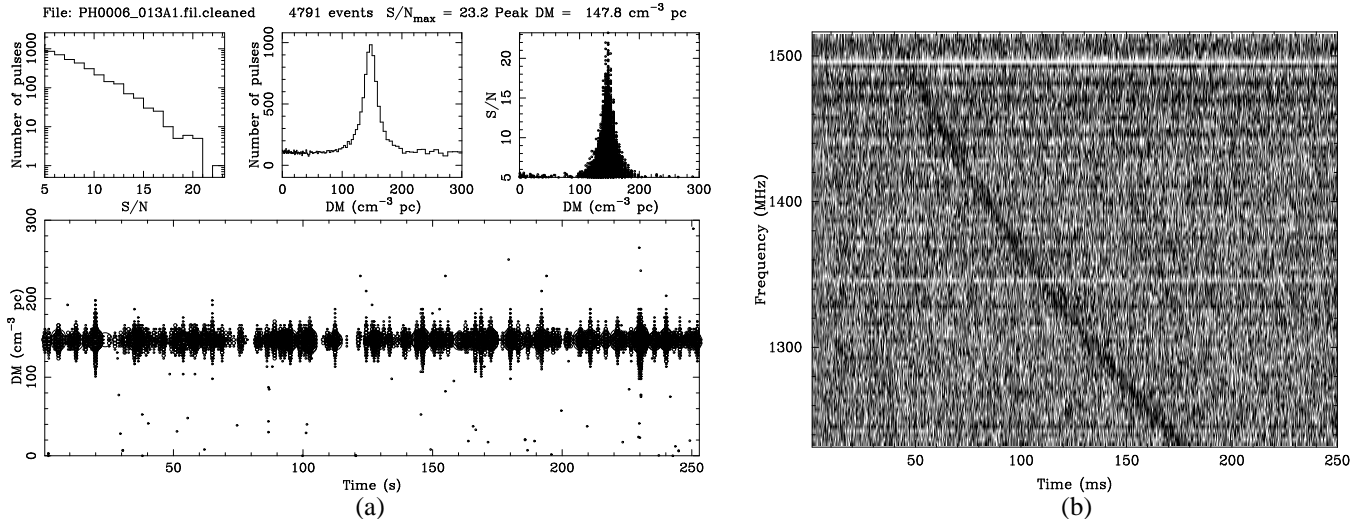


**Figure 1.** Example output of one single-pulse search processing pipeline, showing bright single pulses from PSR J0837–4135 around a DM value of  $147 \text{ cm}^{-3} \text{ pc}$ . The top left panel shows the S/N distribution of the detected pulses, number of pulses versus trial DM (in top center), and S/N as a function of trial DM. The lower plot shows S/N of events as a function of time and trial DM. The size of the circles is linearly proportional to the S/N of each pulse. The dispersive delay in the frequency versus time plot is seen on the right for 250 milliseconds of data.

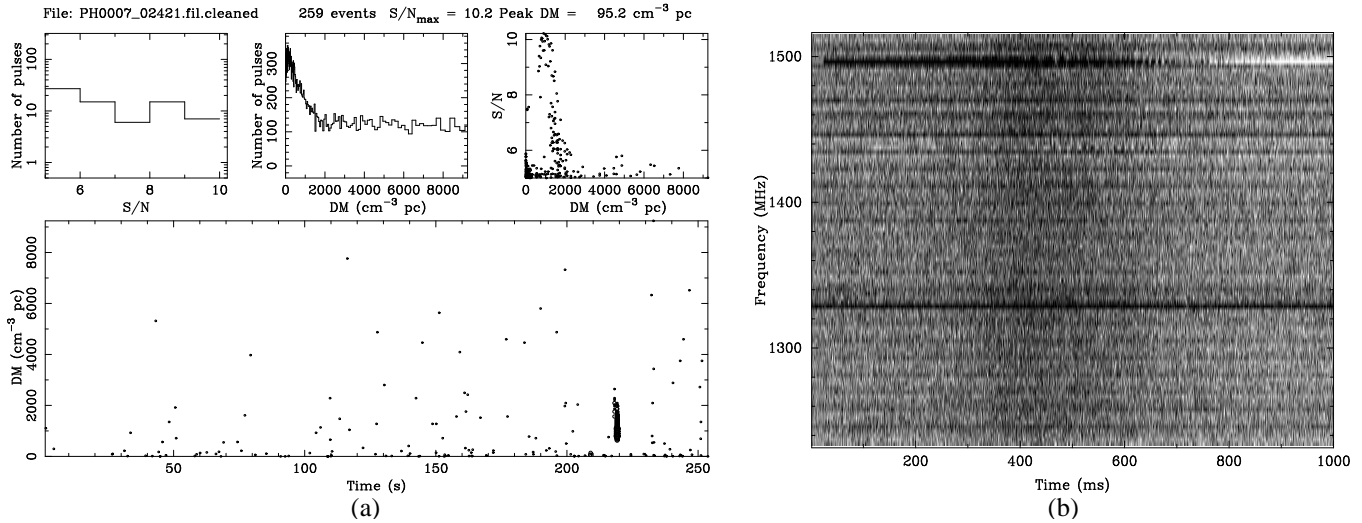


**Figure 2.** The left panel shows a non-astrophysical dispersed burst as seen in the lower plot and a corresponding peak in the S/N versus DM plot. The non-dedispersed data is then plotted corresponding to time of the peak for one second as seen in the right panel here, confirming that it is a false detection.

In our analysis, only one pulse was detected in this observation for PSR J0410–3113, consistent with the non-detection in the periodicity search<sup>3</sup>.

### 3.1 Energy measurements

Integrated profiles for each pulsar were obtained by folding the dedispersed time series using ephemerides available from the ATNF pulsar catalog (Manchester et al. 2005). To construct the pulse energy histograms, the procedure described in Ritchings (1976) is followed. The position and widths of

the on-pulse and off-pulse windows were determined by visual inspection of the integrated pulsar profile. Baseline estimation was done using the off-pulse bins, and was subtracted from the data for each pulse. The total energy for each pulse in the on-pulse window was calculated and is scaled to account for different widths of on and off windows.. The on-pulse data were taken in blocks of about 100 pulses. The on-pulse and off-pulse normalized energies,  $E/\bar{E}$ , were calculated for each block by dividing on-pulse and off-pulse energies within the block by the mean on-pulse energy of that block to account for variations due to interstellar scintillation. The pulse energy histograms were constructed for 10 of the total 17 re-detected pulsars, as shown in Fig. 3, based on the number of pulses detected during the total ob-

<sup>3</sup> The ATNF pulsar catalog can be accessed online at <http://www.atnf.csiro.au/research/pulsar/psrcat>

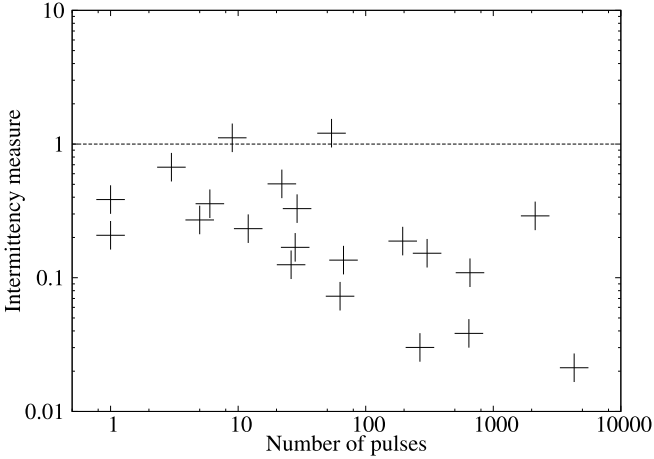


**Figure 4.** Intermittency measure for each pulsar detection in our survey.

servation time. We did not create energy distribution plots for sources with fewer than 100 pulses per observation.

For some pulsars, the on-pulse distribution peaks at the mean energy, as seen for PSR J0742–2822, PSR J0630–2834, PSR J0837–4135, and PSR J0922+0638. In the case of PSR J0742–2822, the energy histograms separate out clearly with no zero energy excess in the ON histogram, suggesting that this pulsar does not null. For other pulsars (PSR J0448–2749, PSR J0828–3417, and PSR J1046+0304), the histograms overlap just because the S/N is low and not necessarily because the pulsar actually nulls. But it is important to note here that the statistics are limited by the relatively short observation time in the survey. So, we did not fit any Gaussians to the histograms since the errors would be large. Even if the pulsar is nulling, there are insufficient pulses to form a distribution for estimation of the nulling fraction in our analysis.

### 3.2 Intermittency measure

The two search algorithms used for pulsar searching show varying levels of efficiency which depend upon the properties of each particular pulsar (McLaughlin & Cordes 2003). Following Deneva et al. (2009), we calculated the intermittency ratio

$$r = \frac{(S/N)_{\text{SP}}}{(S/N)_{\text{per}}} \quad (3)$$

for each pulsar from the S/N value of the single-pulse and periodicity searches and  $r$  is plotted versus the number of periods in  $T_{\text{obs}}$  (see Fig. 4). All the pulsars re-detected in our analysis except PSR J0410–3113 were detected in a previous periodicity search. The pulsars on the upper left have longer periods and the pulsars on the lower right of this plot are millisecond pulsars. Pulsars with  $r > 1$  (PSRs J0726–2612 and J0823+0159) are more likely to be detected with single-pulse searches. PSR J0726–2612, with  $r \sim 1.1$ , has  $P = 3.4$  s and  $\text{DM} = 69$  pc cm $^{-3}$  and PSR J0437–4715, with  $r \sim 0.02$ , has  $P = 5.7$  ms and  $\text{DM} = 2.6$  pc cm $^{-3}$ . These ratios are higher than one would expect in longer surveys, because of the dependence of sensitivity on number of pulses. The integration time for this survey was relatively short (265 s) and

we detected 50% of pulsars from single-pulse search. This can be compared to the PM survey with long integration time (2100 s), in which the single-pulse detections were only about 30% of the total pulsar discoveries from periodicity search (Keane et al. 2010).

## 4 EVENT RATE OF FRBS

Although our analysis did not result in any new FRB detections, it is important to consider the impact of this null result on the FRB event rate,  $\mathcal{R}$ . To put our results into context, we also consider a number of other surveys at Parkes in the calculation below. To constrain  $\mathcal{R}$ , we apply a Bayesian approach which uses the FRB detections in each survey. Using Bayes’ theorem (see, e.g., Wall & Jenkins 2003), the posterior probability density function for  $\mathcal{R}$ , given the detection of  $n$  pulses

$$p(\mathcal{R}|n) \propto p(n|\mathcal{R})p(\mathcal{R}), \quad (4)$$

where  $p(n|\mathcal{R})$  is the likelihood of getting  $n$  detections given some  $\mathcal{R}$  and  $p(\mathcal{R})$  is the prior on the rate of FRBs taken to be uniform. Taking  $n = 0$  from Petroff et al. (2014) and assuming the counting of these rare events as a Poisson process, the likelihood function

$$p(0|\mathcal{R}) = \frac{(\mathcal{R}A_P T_P)^0 \exp(-fRT_P A_P)}{0!}, \quad (5)$$

where  $A_P = 4449$  deg $^2$  and  $T_P = 540$  sec is the total observation time for each pointing. The subscript  $P$  corresponds to the values for Parkes. The numerical factor  $f = (86400 \times 41253)^{-1}$  is inserted to compute  $\mathcal{R}$  in units of bursts day $^{-1}$  sky $^{-1}$ . The posterior probability density of the FRB event rate can be computed as

$$p(\mathcal{R}|0) = K_1 \mathcal{R}^0 \exp(-fRT_P A_P), \quad (6)$$

where  $K_1$  is a normalizing constant which ensures that the above expression integrates over all values of  $\mathcal{R}$  to unity. Integrating this function, we find that the mean FRB rate based on zero FRBs in the HTRU mid-latitude survey is  $\mathcal{R} = 0.22^{+4.5}_{-0.21} \times 10^3$  FRBs day $^{-1}$  sky $^{-1}$ , where the uncertainties represent the 99% confidence interval. To include the FRB detections and null results from subsequent surveys, a similar calculation is performed to determine the FRB event rates for individual surveys as listed in Table 2. The surveys were processed using different search algorithms and therefore the rates need to be modified following the results of Keane & Petroff (2015) in order to combine the individual event rates. As per the response curve shown in Figure 1 of Keane & Petroff (2015), we get the corrected S/N from the use of these algorithms by defining the efficiency factors,  $\eta_{\text{ddall}}$  and  $\eta_{\text{seek}}$ . For **dedisperse\_all**, we find

$$\eta_{\text{ddall}} = \frac{S/N_{\text{dedisperse\_all}}}{S/N_{\text{max}}} = 0.83. \quad (7)$$

and, for **seek**,

$$\eta_{\text{seek}} = \frac{S/N_{\text{seek}}}{S/N_{\text{max}}} = 0.89. \quad (8)$$

The FRB searches we consider in this analysis are the results of reprocessing the Parkes Multibeam (PMPS) survey (Keane et al. (2010, 2011), used **destroy**), the PH sur-

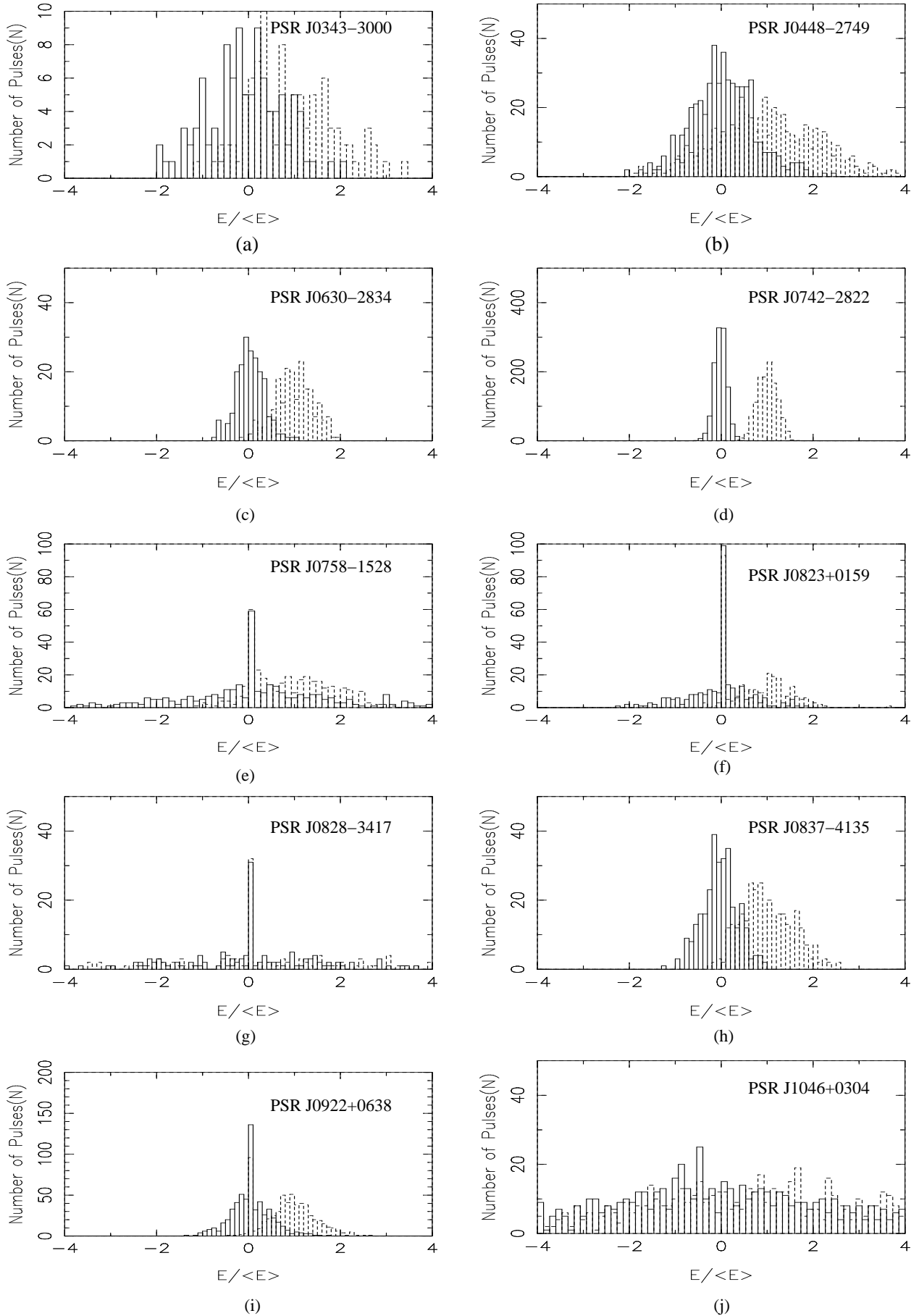


Figure 3. Normalized histograms of on-pulse (dashed) and off-pulse (solid) energies, for 10 of the total 21 re-detected pulsars.

vey (this paper, used `seek`), the Swinburne intermediate and high-latitude (SWIN) surveys (Edwards et al. (2001), Jacoby et al. (2009), Burke-Spolaor & Bannister (2014), used `dedisperse_all`), the HTRU high-latitude (HTRU high) survey (Thornton et al. (2013), Thornton (2013), used `dedisperse_all`), and the HTRU mid-latitude (HTRU mid) survey (Petroff et al. (2015a), used `Heimdall`). In addition to this, the HTRU surveys were carried out using the digital back-end, Berkeley-Princeton-Swinburne Recorder (BPSR), whereas the older Parkes surveys used the analogue filter-bank (AFB). In order to compare all Parkes surveys, the digitization loss factors ( $\beta$ ) depending on the back-end used need to be considered in our analysis. For AFB,  $\beta = 1.25$  and for BPSR,  $\beta = 1.07$  (Kouwenhoven & Voûte 2001). We then insert the efficiency factors into the minimum fluence equation calculated for each processed survey

$$F_{\min} = \frac{\beta T_{\text{sys}}(S/N)_{\min}}{G \eta_{\text{soft}} \sqrt{N_p} \Delta f} \sqrt{w}, \quad (9)$$

where  $T_{\text{sys}}$  is the system temperature,  $G = 0.66$  K/Jy is the telescope gain,  $N_p$  is number of polarizations,  $\Delta f$  is the bandwidth,  $\eta_{\text{soft}}$  is either  $\eta_{\text{seek}}$  or  $\eta_{\text{ddall}}$  depending the survey, and  $w$  is the pulse width equal to the sampling time when calculating the minimum fluence. The HTRU mid-latitude survey has the lowest minimum fluence as can be seen in Table 2. The event rates of other surveys are scaled to this lowest  $F_{\min}^{-3/2}$  which is the simplest model assuming a uniform distribution of standard-candle FRBs in Euclidean geometry. The modified event rates are shown in Fig. 5. Combining all these individual rate estimates, Fig. 6 shows our current best estimate of  $\mathcal{R}$ . The mean FRB rate from this distribution is  $4.4_{-3.1}^{+5.2} \times 10^3$  FRBs day $^{-1}$  sky $^{-1}$  for sources with a fluence above 4.0 Jy ms at 1.4 GHz, where the uncertainties represent a 99% confidence interval. To demonstrate that this rate is consistent with all the surveys considered here, we list in Table 2 the predicted upper and lower bounds on the number of FRBs expected in each survey which use these 99% confidence intervals on  $\mathcal{R}$  and scale it back to each survey's fluence limit. In addition, we make predictions for future analyses of the Perseus Arm (PA) pulsar survey (Burgay et al. 2013) and HTRU low-latitude survey (Thornton 2013).

The event rate is estimated assuming FRBs are uniformly distributed on the sky. We now consider the impact of this assumption. The Galactic effects such as dispersion in the ISM, scattering in the ISM, scintillation, and sky temperature can limit the sensitivity of a survey. Following the discussion in Petroff et al. (2014) about decreased sensitivity to FRBs at  $|b| \leq 15^\circ$ , we compare the sensitivity based on sky coverage for the Parkes surveys considered in our calculations. The non-Galactic DM contribution at high latitudes range between 520 and 1070 cm $^{-3}$  pc. The Galactic dispersion at these latitudes is only about 50 cm $^{-3}$  pc, whereas the average Galactic dispersion at intermediate latitudes and near the Galactic center are 380 cm $^{-3}$  pc and 1780 cm $^{-3}$  pc respectively. The FRB pulses with an additional non-Galactic DM contribution at these lower latitudes would still be recovered in the surveys considered above as they have been searched to a sufficient DM, with the maximum trial DM in each of these surveys being  $> 2000$  cm $^{-3}$  pc.

The average sky temperature values for four of these

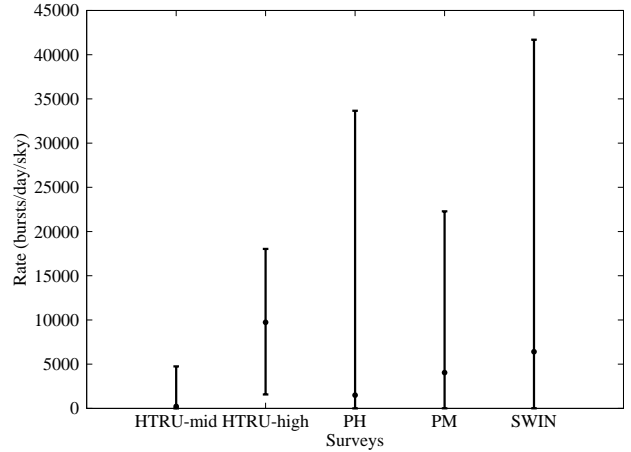


**Figure 5.** The modified FRB event rates based on individual survey results and corrected for detection sensitivity based on the search algorithms and the backend used.

surveys range between 0.85 K to 3.18 K and about 6.14 K for the PMPS survey (Burke-Spolaor & Bannister 2014). Sky temperature is therefore not a significant factor in limiting the sensitivity when comparing these surveys.

FRBs discovered so far (except FRB 110220) show few effects of scattering (see, e.g., Lorimer et al. 2013). Petroff et al. (2014) determined that more than 85% of survey pointings in the intermediate latitude survey are still sensitive to FRB signals even in the presence of strong scattering in the ISM near the Galactic center. This percentage will differ for AFB surveys as the number of channels, sampling time, and digitization factors are different but is still small compared to overall uncertainty in the FRB event rate at this point.

Petroff et al. (2014) analyzed how the combination of these effects limits sensitivity for survey pointings and determined that a simulated FRB pulse with properties similar to the FRBs in Thornton (2013) falls below the detection threshold in only 14% of all intermediate latitude pointings assuming no scattering in the ISM. We combine the individual rates since the sensitivity variations between AFB and BPSR are within the uncertainty of rate of FRBs. Petroff et al. (2014) argue that since the percentage of pointings no longer sensitive to FRB pulses decreases to 14%, the null result is discrepant with the original predictions based on a higher event rate. Although, if the event rate of FRBs is much lower than previous estimates, it still explains the null result at intermediate latitudes (Table 2). Therefore, we argue that the lack of detections at intermediate latitudes and the null result in our analysis of a high-latitude survey are likely to be due to a lower FRB rate and does not necessarily imply a dearth of FRBs at intermediate latitudes.

## 5 CONCLUSIONS

We have presented the results of a single-pulse search of the PH pulsar survey. We re-detected 20 of the previously known pulsars reported by Burgay et al. (2006) and detected one RRAT. Out of these 21 re-detections, we have constructed pulse energy histograms for 10 pulsars for which the observed number of pulses was more than 100. For PSR

**Table 2.** Survey parameters, FRB detections, event rates and predicted numbers of FRBs for multibeam pulsar surveys carried out at Parkes. The survey abbreviations are listed in the text. For each survey, we provide the dwell time ( $T$ ), area covered ( $A$ ), bandwidth ( $\Delta f$ ), digitization factor ( $\beta$ ), efficiency factor ( $\eta$ ), sampling time ( $t_{\text{samp}}$ ), system temperature ( $T_{\text{sys}}$ ), minimum fluence ( $F_{\text{min}}$ ), number of FRBs found ( $N_{\text{FRBs}}$ ), estimated FRB event rate ( $\mathcal{R}$ ), and the modified FRB event rate ( $\mathcal{R}_{\text{mod}}$ ). Using the combined FRB event rate, we give the number of FRBs expected to be found ( $N_{\text{expected}}$ ), as well as lower and upper bounds on this expected number ( $N_{\text{lower}}$  and  $N_{\text{upper}}$ ).

Parameter	HTRU High	HTRU Mid	HTRU Low	SWIN	PA	PMPS	PH
Dwell time $T$ (s)	270	540	4300	265	2100	2100	265
Area $A$ (deg <sup>2</sup> )	21671.6	4448.8	769.5	7264.3	599.3	2097.4	3979.5
Bandwidth $\Delta f$ (MHz)	400	400	400	288	288	288	288
Digitization $\beta$	1.07	1.07	1.07	1.25	1.25	1.25	1.25
Efficiency $\eta_{\text{soft}}$	0.83	1.0	1.0	0.83	1.0	1.0	0.75
Sampling time $t_{\text{samp}}$ (ms)	0.064	0.064	0.064	0.125	0.125	0.25	0.125
System temperature $T_{\text{sys}}$ (K)	29.0	30.5	35.5	29.5	29.2	33.6	29.0
Fluence $F_{\text{min}}$ (Jy ms)	4.6	4.0	4.6	8.9	7.3	11.9	8.2
$N_{\text{FRBs}}$	5	0	—	1	—	1	0
$\mathcal{R}$ (10 <sup>3</sup> FRBs d <sup>−1</sup> sky <sup>−1</sup> )	$7.9^{+14.6}_{-6.6}$	$0.22^{+4.5}_{-0.21}$	—	$1.9^{+10.2}_{-1.8}$	—	$0.81^{+4.5}_{-0.8}$	$0.5^{+10.1}_{-0.4}$
$\mathcal{R}_{\text{mod}}$ (10 <sup>3</sup> FRBs d <sup>−1</sup> sky <sup>−1</sup> )	$9.7^{+18.0}_{-8.2}$	$0.22^{+4.5}_{-0.21}$	—	$6.2^{+34.1}_{-6.2}$	—	$4.1^{+22.3}_{-4.0}$	$1.5^{+33.7}_{-1.4}$
$N_{\text{expected}}$	2	3	3	1	1	1	0
$N_{\text{upper}}$	5	6	7	2	1	2	1
$N_{\text{lower}}$	1	1	1	0	0	0	0

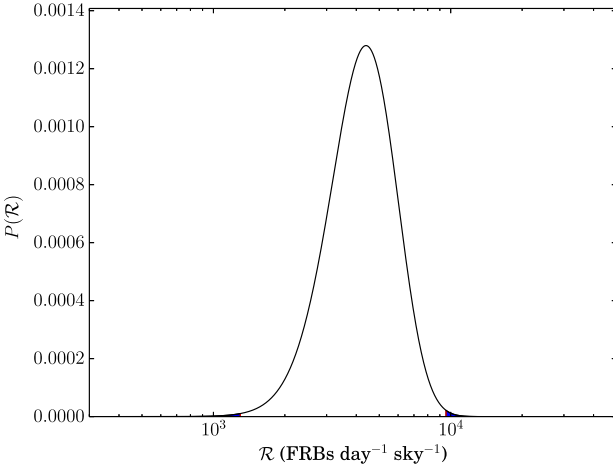


**Figure 6.** The combined posterior PDF of the FRB event rate taking into account all the published Parkes survey results carried out to date and correcting for detection sensitivity based on the search algorithms used and the backend used. The all-sky event rate for sources with a fluence above 4.0 Jy ms is  $\mathcal{R} = 4.4^{+5.2}_{-3.1} \times 10^3$  FRBs day<sup>−1</sup> sky<sup>−1</sup>.

J0742–2822, the on-pulse and off-pulse histograms separate out clearly, suggesting it does not null over the observing span. The observation time, being relatively short, is insufficient for estimation of the nulling fraction. We demonstrated, using a Bayesian approach that the lack of FRB detections, and detection rates in other surveys, is consistent with an all-sky FRB event rate  $\mathcal{R} = 4.4^{+5.2}_{-3.1} \times 10^3$  FRBs day<sup>−1</sup> sky<sup>−1</sup>, for sources with a fluence above 4.0 Jy ms at 1.4 GHz, where the uncertainties represent a 99% confidence interval. This event rate takes into account the decrease in detection sensitivity as a result of the search algorithms used in the analysis and the differ-

ent backends used in these surveys. We argue that previous suggestions of a dearth of FRBs at intermediate Galactic latitudes is likely to be a result of the assumption of a higher event rate. The revised event rate found here is in good agreement with Keane & Petroff (2015) who estimated  $\mathcal{R} \sim 2500$  FRBs day<sup>−1</sup> sky<sup>−1</sup>. We concur with these authors that a larger sample of FRBs is required to more meaningfully constrain the rate.

## 6 ACKNOWLEDGEMENTS

This work was partially supported by the Astronomy and Astrophysics Division of the National Science Foundation via grant AST-1309815. We thank the referee for helpful comments on the manuscript.

## REFERENCES

- Burgay, M., Joshi, B. C., D’Amico, N., et al. 2006, MNRAS, 368, 283
- Burgay, M., Keith, M. J., Lorimer, D. R., et al. 2013, MNRAS, 429, 579
- Burke-Spolaor, S., Bailes, M., Ekers, R., Macquart, J.-P., & Crawford, F., III 2011, ApJ, 727, 18
- Burke-Spolaor, S., Bailes, M., Johnston, S., et al. 2011, MNRAS, 416, 2465
- Burke-Spolaor S., Bannister K. W., 2014, ApJ, 792, 19
- Cordes, J. M., & Lazio, T. J. W. 2002, arXiv:astro-ph/0207156
- Cordes, J. M., & McLaughlin, M. A. 2003, ApJ, 596, 1142
- Cordes, J. M., Lazio, T. J. W., & McLaughlin, M. A. 2004, New Astronomy Review, 48, 1459
- Deneva, J. S., Cordes, J. M., McLaughlin, M. A., et al. 2009, ApJ, 703, 2259
- Dennison, B. 2014, MNRAS, 443, L11

Eatough, R. P., Keane, E. F., & Lyne, A. G. 2009, MNRAS, 395, 410

Edwards, R. T., Bailes, M., van Straten, W., & Britton, M. C. 2001, MNRAS, 326, 358

Falcke, H., & Rezzolla, L. 2014, A&A, 562, AA137

Jacoby, B. A., Bailes, M., Ord, S. M., Edwards, R. T., & Kulkarni, S. R. 2009, ApJ, 699, 2009

Kashiyama, K., Ioka, K., & Mészáros, P. 2013, ApJL, 776, LL39

Keane, E. F., Ludovici, D. A., Eatough, R. P., et al. 2010, MNRAS, 401, 1057

Keane, E. F., Kramer, M., Lyne, A. G., Stappers, B. W., & McLaughlin, M. A. 2011, MNRAS, 415, 3065

Keane, E. F., Stappers, B. W., Kramer, M., & Lyne, A. G. 2012, MNRAS, 425, L71

Keane, E. F., & Petroff, E. 2015, MNRAS, 447, 2852

Kouwenhoven, M. L. A., & Voûte, J. L. L. 2001, A&A, 378, 700

Lazio, T. J. W. 2012, Square Kilometre Array: Paving the Way for the New 21st Century Radio Astronomy Paradigm, 53

Levin L., 2012, PhD thesis, Swinburne University of Technology

Lipunov, V. M., & Pruzhinskaya, M. V. 2014, MNRAS, 440, 1193

Loeb, A., Shvartzvald, Y., & Maoz, D. 2014, MNRAS, 439, L46

Lorimer, D. R., & Kramer, M. 2004, Handbook of pulsar astronomy, by D.R. Lorimer and M. Kramer. Cambridge observing handbooks for research astronomers, Vol. 4. Cambridge, UK: Cambridge University Press, 2004

Lorimer, D. R., Bailes, M., McLaughlin, M. A., Narkevic, D. J., & Crawford, F. 2007, Science, 318, 777

Lorimer, D. R., Karastergiou, A., McLaughlin, M. A., & Johnston, S. 2013, MNRAS, 436, L5

Luan, J., & Goldreich, P. 2014, ApJL, 785, LL26

Manchester, R. N., Hobbs, G. B., Teoh, A., & Hobbs, M. 2005, AJ, 129, 1993-2006 (2005), astro-ph/0412641

Maoz, D., Loeb, A., Shvartzvald, Y., et al. 2015, arXiv:1507.01002

McLaughlin, M. A., & Cordes, J. M. 2003, ApJ, 596, 982

McLaughlin, M. A., Lyne, A. G., Lorimer, D. R., et al. 2006, Nature, 439, 817

Petroff, E., van Straten, W., Johnston, S., et al. 2014, ApJL, 789, LL26

Petroff, E., Bailes, M., Barr, E. D., et al. 2015, MNRAS, 447, 246

Petroff, E. et al. 2015, arXiv:1504.02165

Pietka, M., Fender, R. P., & Keane, E. F. 2015, MNRAS, 446, 3687

Popov, S. B., & Postnov, K. A. 2013, arXiv:1307.4924

Ravi, V., Shannon, R. M., & Jameson, A. 2014, arXiv:1412.1599

Ritchings, R. T. 1976, MNRAS, 176, 249

Spitler, L. G., Cordes, J. M., Hessels, J. W. T., et al. 2014, ApJ, 790, 101

Thornton, D., Stappers, B., Bailes, M., et al. 2013, Science, 341, 53

Thornton D. P. G., 2013, PhD thesis, The University of Manchester

Totani, T. 2013, Publications of the Astronomical Society of Japan, 65, L12

Wall, J. V., Jenkins, C. R., Ellis, R., et al. 2003, Practical statistics for astronomers, by J.V. Wall and C.R. Jenkins. Cambridge observing handbooks for research astronomers, vol. 3. Cambridge, UK: Cambridge University Press, 2003

## 7 APPENDIX

Levin (2012) describes the the algorithm which accounts for the amount of pulse broadening caused by the size of the previous DM step and then determines the next trial DM. The appropriate step size is computed from the effective pulse width ( $w_{\text{eff}}$ ), which is a quadrature sum of the intrinsic pulse width ( $t_{\text{in}}$ ), the smearing due to scattering ( $t_{\text{scatt}}$ ), dispersion smearing within each frequency channel ( $t_{\text{DM}}$ ), sampling time of a particular survey ( $t_{\text{samp}}$ ), and smearing across all frequency channels due to the dispersion measure step size ( $t_{\Delta\text{DM}}$ )

$$w_{\text{eff}} = \sqrt{t_{\text{in}}^2 + t_{\text{scatt}}^2 + t_{\text{samp}}^2 + t_{\text{DM}}^2 + t_{\Delta\text{DM}}^2}, \quad (10)$$

where, for frequencies in GHz and DM in units of  $\text{cm}^{-3} \text{ pc}$ ,

$$t_{\text{DM}} = 8300 \text{ s} \left( \frac{\Delta f \text{ DM}}{f^3} \right) \quad (11)$$

and

$$t_{\Delta\text{DM}} = 8300 \text{ s} \left( \frac{n_{\text{chan}} \Delta f \Delta\text{DM}}{4 f^3} \right). \quad (12)$$

Here  $n_{\text{chan}}$  is the number of frequency channels and  $\Delta\text{DM} = \text{DM} - \text{DM}'$ . Since 4 samples are packed per 64-bit word, the equation is divided by a factor of 4. Since the total pulse width smearing of 25% is chosen, the pulse broadening fraction due to the DM step is  $\epsilon = 1.25$ . Then the effective pulse width at the new trial DM, with respect to the last trial DM' is

$$(w_{\text{eff}}|_{\text{DM}}) = \epsilon (w_{\text{eff}}|_{\text{DM}'}) \quad (13)$$

Solving for DM by equating  $w_{\text{eff}}$  at the new trial value, DM, with respect to the last trial value, DM',

$$\text{DM} = \frac{b^2 \text{DM}' + \sqrt{-a^2 b^2 \text{DM}'^2 + a^2 c + b^2 c}}{a^2 + b^2}, \quad (14)$$

where

$$a = 8300 \text{ s} \frac{\Delta f \text{ DM}}{f^3}, \quad (15)$$

$$b = t_{\Delta\text{DM}} = 8300 \text{ s} \frac{n_{\text{chan}} \Delta f \Delta\text{DM}}{4 f^3}, \quad (16)$$

and

$$c = \epsilon^2 (t_{\text{in}}^2 + t_{\text{scatt}}^2 + t_{\text{samp}}^2 + t_{\text{DM}}^2) - t_{\text{samp}}^2 - w_{\text{in}}^2. \quad (17)$$

The DM values are obtained using Equation 14 where DM step is finely spaced for small values of DM. For higher DM values, pulse smearing is greater than the sampling time and hence the temporal resolution is decreased giving DM channels that are spaced more coarsely.